Published in final edited form as:
J Phys Chem B. 2009 February 26; 113(8): 2477–2485. doi:10.1021/jp808182y.

Determination of the Structure Form of the Fourth Ligand of Zinc in Acutolysin A Using Combined Quantum Mechanical and Molecular Mechanical Simulation

Emilia L. Wu[†], **Kin-Yiu Wong**[‡], **Xin Zhang**[†], **Keli Han**[*,†], and **Jiali Gao**[*,‡]
Dalian Institute of Chemical Physics, Chinese Academy of Sciences, Dalian, P. R. China 116023, and Department of Chemistry, Digital Technology Center and Minnesota Supercomputing Institute, University of Minnesota, Smith Hall, 207 Pleasant Street SE, Minneapolis, Minnesota 55455

Abstract

Acutolysin A, which is isolated from the snake venom of Agkistrodon acutus, is a member of the SVMPs subfamily of the metzincin family, and it is a snake venom zinc metalloproteinase possessing only one catalytic domain. The catalytic zinc ion, in the active site, is coordinated in a tetrahedral manner with three imidazole nitrogen atoms of histidine and one oxygen atom. It is uncertain whether this oxygen atom is a water molecule or a hydroxide ion just from the three-dimensional X-ray crystal structure. The identity of the fourth ligand of zinc is theoretically determined for the first time by performing both combined quantum mechanical and molecular mechanical (QM/MM) simulation and high-level quantum mechanical calculations. All of the results obtained indicate that the fourth ligand in the active site of the reported X-ray crystal structure is a water molecule rather than a hydroxide anion. On the basis of these theoretical results, we note that the experimental observed pH dependence of the proteolytic and hemorrhagic activity of Acutolysin A can be attributed to the deprotonation of the zinc-bound water to yield a better nucleophile, the hydroxide ion. Structural analyses revealed structural details useful for the understanding of acutolysin catalytic mechanism.

Introduction

Zinc is essential to all forms of life.[1−9] Zinc enzymes appear to be the most abundant and well studied both experimentally and theoretically among all the naturally found metalloproteins.[10] There are approximately 300 zinc enzymes, with representatives known for each of the fundamental enzyme classes (oxidoreductases, transferases, hydrolases, lyases, isomerases, and ligases). Much of the importance of zinc enzymes derives from their peptidase and amidase activity involving the cleavage of $R_1C(O)–NH(R_2)$ amide bonds. In addition, zinc enzymes play an important role in the cleavage of the P–OR bond in phosphates, $[(RO)PO_3]^{2-}$ and $[(RO)_2PO_2]^-$, as exemplified by their nuclease activity pertaining to the hydrolysis of DNA and RNA.[1] Therefore, it is evident that zinc plays multifaceted roles in biological systems, and a detailed understanding of these roles requires correspondingly detailed enzyme structural information.

* To whom correspondence should be addressed. klhan@dicp.ac.cn. Tel.: +86 0411 84379293. Fax: +86 0411 84675584..
[†]Chinese Academy of Sciences.
[‡]University of Minnesota.

Supporting Information Available: Figure S1, plots of the temperature versus the simulation time: (a) for 1bsw_water, and (b) for 1bsw_hydroxide. Figure S2, plots of the potential energy versus the simulation time: (a) for 1bsw_water, and (b) for 1bsw_hydroxide. The information is available free of charge via the Internet at http://pubs.acs.org.

Many new interesting zinc enzymes have been identified and structurally characterized in the past few years. In the most common structural motif of zinc enzymes, a few functional residues seem to be most important for catalysis: the zinc ion, a zinc-coordinated oxygen atom, and a carboxylate side chain.[4] Since the resolution of the X-ray structure is not sufficiently high, the positions of the hydrogen atoms are not available. Consequently, the identity of the oxygen coordination in the form of a water molecule or a hydroxide ion is not clearly defined. Despite decades of intensive research, some doubts concerning the protonation state of functional active site residues still remain.[4] In this regard, Zhan et al. have theoretically determined the identity of the bridging oxygen in zinc-substituted phosphotriesterase and the study indicates that the critical bridging oxygen exists in the form of hydroxide ion in this dinuclear metallopeptidase.[11] Our interest is to determine the structure form of the zinc-coordinated oxygen atom in the monozinc enzyme of Acutolysin A.[12]

Snake venoms are a rich source of zinc-dependent metalloproteinases.[13–15] Apart from playing an important role in the digestion of prey tissues, these enzymes also participate in the pathophysiology of envenoming by inducing local and systemic bleeding,[13,16,17] as well as other tissue-damaging activities and hemostatic alterations.[13,16,18] Acutolysin A is a 22 kDa hemorrhagic toxin isolated from the snake venom of *Agkistrodon acutus*.[12] It can be classified into the P-I subclass of snake venoms metalloproteinases (SVMP) possessing only one catalytic domain, and it is also a member of the matrix metalloproteinases (MMP) superfamily for the similarity of the constituent domains.[19] The crystal structure of Acutolysin A is shown in Figure 1 using 1bsw.pdb of Gong et al.[12] The catalytic zinc ion is coordinated in a tetrahedral manner with one oxygen atom anchoring to an intermediate glutamic acid residue (Glu143) and three imidazole $N^{\epsilon 2}$ atoms of His142, His146, and His152 in the highly conserved sequence $H_{142}E_{143}$-$XXH_{146}XXGXXH_{152}$. This oxygen atom, which is located in the neighborhood of the carboxylate group of the glutamate residue, is considered to be a base for nucleophilic attack on the carbonyl carbon atom of the sensitive peptide bond.[12] Here we theoretically determine the identity of this critical ligand by performing both combined quantum mechanical and molecular mechanical (QM/MM) simulation on the solvated protein and high-level quantum mechanical calculations on simplified models of the active site. At present, the cleavage patterns of many SVMPs on basement membrane proteins are largely unknown,[20] and the detailed structural data of the active site are essential to fully understand the catalytic and hemorrhagic mechanism. In addition, insights gained from this structural study also facilitate the rational design of potential drugs to treat diseases where matrix metalloproteinases have been implicated, e.g., arthritis and tumor metastasis.21

Modeling the behavior of a zinc atom and its ligands is a challenging task with a pure MM force field.[22–25] Indeed, its large positive charge can result in substantial polarization effects, local geometric changes, and coordination number changes.[22,23] In this work, molecular dynamics simulation was carried out to explore equilibrium structural information and dynamic behavior of the active site of Acutolysin A using the QM/MM potential. QM/MM methods solve these problems by treating the metal ion and its ligands quantum mechanically while treating the surrounding environment with a force field. In this approach, polarization of the metal ion and its ligands can be effectively dealt with since it is explicitly included in the QM/MM model. Furthermore, the dynamics of the coordination sphere is included as well as the ability to undergo coordination changes.[23]

Computational Details

A. Modeling

To determine the form of the fourth ligand of zinc, simulations were carried out on each of the alternative zinc-ligand structures: one with water and the other with the hydroxide anion. The X-ray crystal structure of Acutolysin A determined at 1.95 Å resolution (Protein Data Bank

code 1BSW) was used as the starting geometry for all simulations.[12] All the water molecules originally determined in the X-ray crystal structure were kept. The coordinates for all hydrogen atoms were generated using the HBUILD facility in CHARMM, and the protonation states for ionizable residues were set corresponding to neutral pH. Thus, histidine residues were modeled as neutral or protonated residues on the basis of possible hydrogen bond interactions deduced from the X-ray crystallographic structure.26 The resulting systems have a net charge of –2e or –3e for the case of the ligand being water and hydroxide, respectively. The system containing water molecule was neutralized by adding four sodium cations and two chloride anions, while the hydroxide system was neutralized by adding five sodium cations and two chloride anions. The final protein structures were solvated with cubic boxes of water molecules using the package of Visual Molecular Dynamics.27 The initial dimension of the boxes was 62 × 62 × 62 $Å^3$, which ensures that all the protein atoms are at least 10 Å away from the edges of the boxes. Water molecules within 2.5 Å of any non-hydrogen atoms of the protein or existing water were removed. The final model contains 24 055 atoms of which 3019 are protein atoms for the system containing water molecule.

B. Combined QM/MM Potential

The method of combined QM/MM potentials has been reviewed elsewhere.[28–31] Here, we provide a brief summary of the basic framework of this method for completeness. For a hybrid QM and MM system, the effective Hamiltonian is given by

$$\widehat{H}_{\text{eff}}=\widehat{H}^{0}_{\text{qm}}+\widehat{H}_{\text{qm/mm}}+\widehat{H}_{\text{mm}} \tag{1}$$

where $\widehat{H}^{0}_{\text{qm}}$ is the Hamiltonian for the QM subsystem, $\hat{H}_{\text{mm}}$ is the molecular mechanical potential of the MM subsystem, and $\hat{H}_{\text{qm/mm}}$ describes the interactions between the quantal and classical parts of the system. The interaction Hamiltonian can be further divided into an electrostatic term and a van der Waals component,[29,30] in which the former accounts for the interactions between the electrons and nuclei of the QM subsystem and the partial atomic charges of the MM sites, and the latter is modeled by a Lennard-Jones form

$$\widehat{H}^{\text{vdW}}_{\text{qm/mm}}=\sum_{s=1}^{S}\sum_{m=1}^{M}4\varepsilon_{sm}\left[\left(\frac{\sigma_{sm}}{R_{sm}}\right)^{12}-\left(\frac{\sigma_{sm}}{R_{sm}}\right)^{6}\right] \tag{2}$$

where M and S are respectively the total number of QM atoms and MM interaction sites, and R_{sm} is the distance of the QM atom m from the MM site s. The combining rules for eq 2 are $\sigma_{sm} = (\sigma_s + \sigma_m)/2$ and $\varepsilon_{sm} = (\varepsilon_s\varepsilon_m)^{1/2}$, where σ_i and ε_i are empirical parameters for atom i. Standard force field parameters are used for σ_s and ε_s,[32] whereas van der Waals parameters for the QM subsystem (σ_m and ε_m) can be optimized to obtain the best QM-MM interactions in comparison with experimental values or high-level ab initio calculation.[33,34]

We have adopted the semiempirical parametrized model 3 (PM3) method[35] for the description of the QM region due to the huge computational cost of ab initio or DFT methods. Semiempirical methods, although less systematic than high-level ab initio models that include electron correlation, can still provide important insights, and have been successfully used in numerous enzymatic reactions by several groups.[23,36–42]

In the combined QM/MM treatment, the atoms in the inner coordination sphere of the zinc ion are included in the QM representation. We have used the generalized hybrid orbital (GHO) method to treat the interface between the QM and the MM region,[43] and the C_β atoms of the three histidine residues (His142, His146, and His152) were defined as the GHO boundary

atoms. The rest of the enzyme residues and water molecules are described, respectively, by the CHARMM22 force field[32] and the three point charge TIP3P model.44 A schematic representation of the QM/MM partitioning of the system is shown in Figure 1. A total of 28 or 27 atoms are included in the QM region for the case of the ligand being water and hydroxide, respectively.

C. Molecular Dynamics Simulation

To remove close contacts and highly repulsive orientations of the initial protein–solvent system, we first performed 1500 steps of energy minimization for all water molecules and counterions using the adopted-basis set Newton–Raphson (ABNR) method in CHARMM-version c33, with the protein atoms held fixed. [45] This was followed by 5 ps of molecular dynamics for waters and counterions to allow the solvent molecules to equilibrate, and the temperature was brought up from 200 to 298.15 K. Subsequently, by fixing the atoms in QM region and all the waters and counterions, the protein atoms were minimized using 500 steps of the ABNR method, then another 2 ps molecular dynamics was carried out for these protein atoms with the temperature raised from 200 to 298.15K. Finally, the entire system was heated up from 200 to 298.15 K for 2 ps with all the constraints removed and then was further equilibrated at 298.15 K for another 10 ps with the QM/MM simulation. After the above 19 ps of heating equilibration, the QM/MM simulation of the final system was kept running until the equilibration time of the root-mean-square deviation (rmsd) of MD structure from the X-ray structure is more than 500 ps. The total simulation times are 1 and 1.5 ns for the case of the fourth ligand being water and hydroxide, respectively, and the trajectories saved during the last 100 ps production simulation were collected for structural analysis.

Both the MM and QM/MM simulations were carried out using periodic boundary conditions and the isothermal–isobaric (NPT) ensemble at 298.15 K and 1 atm. In the present study, a spherical cutoff distance of 12 Å was used for the nonbonded interactions generation along with a switch function in the region 11-12 Å to feather the interaction energy to zero. The nonbonded pair list and the image list were built on the basis of group separations, and they were updated every 25 steps. During an image update, the distant solvent molecules were replaced by a close image, and the group of image atoms within the cutoff distance of the primary atoms was updated. We used the leapfrog integration scheme[46] to propagate the equations of motion with a time step of 1 fs and with the extended system constant pressure and temperature algorithm implemented in charmm.47–49 All the bond lengths and bond angles involving hydrogen atoms were constrained by the SHAKE algorithm,50 and the dielectric constant was set to 1.[26]

D. High-Level QM calculation

High-level quantum chemical calculations were carried out on two simplified active site models by use of the Gaussian0351 program, one with water molecule and the other with hydroxide ion. The simplified models are composed of all the atoms in the QM region and GHO boundary atoms, which are saturated with hydrogen atoms. The geometries were fully optimized by employing density functional theory (DFT) using Beck's three-parameter hybrid exchange functional and the Lee-Yang-Parr correlation functional (B3LYP)52,53 with three different basis sets, 6-31+G(d,p), 6-31++G(d,p), and 6-31++G(2d,2p). Previous study of Dudev et al. indicates that the B3LYP/6-31++G(2d,2p) calculations are well suited for evaluating the geometries and interaction free energies of complexes between divalent cations and oxygen- and nitrogen-containing ligands.54–56 Finally, the corresponding vibrational frequencies were evaluated at the optimized geometries to verify their true stability.11

Results and Discussion

The key advantage of molecular dynamics is to sample the protein conformational space. Although the time scale is still generally limited to the submicrosecond range, even this period of time may provide substantial insight into processes that occur in biological systems such as proteins.[57] We have analyzed the simulation trajectories and have followed several geometry parameters that characterize the protein of Acutolysin A. For simplification, 1bsw_water and 1bsw_hydroxide will hereafter be referred to as the simulations containing water or hydroxide ion as the fourth ligand of zinc, respectively. Before sampling the geometry parameters from the trajectories, we consider both the 1bsw_water and 1bsw_hydroxide simulations are equilibrated because of the small values of the fluctuation in temperature (Figure S1) and potential energy (Figure S2). The temperature remains stable around 298.15 K. The potential energy decreased in the beginning of the simulations, then leveled off in less than 100 ps, suggesting that the relaxation is complete and the equilibrium has been reached.

Depicted in Figure 2 are plots of root-mean-square deviations (RMSDs) of the protein backbone atoms, atoms within 10 Å of zinc, as well as atoms in QM region from the initial X-ray structure (PDB ID 1BSW) over the course of the simulation. Each system is simulated until the equilibration time of rmsd exceeding 500 ps. The rmsd of atoms in the QM region exhibits a shift at around 200 ps in 1bsw_water simulation, and after 300 ps the structure rebound to its original relaxed conformation till the end of the 1 ns simulation. The smaller rmsd of Zn^{2+} and its ligands (QM region), as compared with the backbone rmsd, indicate that the metal-binding site is less mobile than the rest of the protein. While the structure of atoms in QM region of 1bsw_hydroxide system oscillates between two alternative conformations, after 800 ps the rmsd reaches a plateau, which indicates that the conformation relaxes to a much different one in comparison with X-ray structure. These conformation fluctuations reflect the changes of hydrogen-bonding patterns in the second coordination shell, which will be illustrated below.

The selected simulated internuclear distances versus the simulation time between atoms in the active site are illustrated in Figure 4, and atom name definition is shown in Figure 3. D1 is the distance between coordinate oxygen atom (water or hydroxide ion) and Zn^{2+}, and D2, D3, and D4 are distances between zinc and the other three ligands. D5 and D6 are those between the ligand oxygen atom (water or hydroxide ion) and carboxylate oxygen atoms of Glu143. Compared with D5 and D6, the distances of D1, D2, D3, and D4 of both simulations have not changed considerably and have been well equilibrated in the simulations. Corresponding results of average distance over the last 100 ps with standard deviation are shown in Table 1. The time-average value of Zn^{2+}–O (D1) for the 1bsw_water simulation, 2.18 Å in Table 1, is in excellent agreement with the experimental value of 2.24 Å, while the simulation with the structure containing the coordinate hydroxide ion produces a very different result. In 1bsw_hydroxide simulation the time-average Zn^{2+}–O distance quickly converged to the value of 1.94 Å, which is qualitatively different from the experimental data. The distances between zinc and three other coordinate nitrogen atoms (D2, D3, and D4) of the 1bsw_water system are also slightly closer to the experimental structure than those of the 1bsw_hydroxide system. Comparison of the calculated structures of 1bsw_water and 1bsw_hydroxide indicates that the hydroxide ligand simulation shortens the Zn-O bond, while lengthening the average Zn-N bond length, which is consistent with the study of Bergquist et al.[58] Though D5 and D6 in 1bsw_water simulation have relative big deviation from the X-ray structure, these two distances are more reasonable than those in 1bsw_hydroxide simulation. Therefore, these inter-nuclear distances from the MD simulations indicate that the fourth ligand in the X-ray structure is a water molecule instead of a hydroxide ion.

MD average rmsd and standard deviations from the experimental structure for three atom sets, backbone atoms (S1), atoms within 10 Å of zinc (S2), and atoms in QM region (S3), are reported

in Table 2. As can be seen from this table, the average values of rmsd are smaller in 1bsw_water simulation than those in the 1bsw_hydroxide simulation for all these three atom sets, and the average rmsd of atoms in QM region (S3) of 1bsw_hydroxide system is twice as that of the 1bsw_water system. Obviously, the starting X-ray structure is much more different from the equilibrated structure in the 1bsw_hydroxide simulation than that in the 1bsw_water simulation. In other words, the fourth coordinate oxygen atom of zinc in the X-ray structure is from a water molecule.

Besides the above QM/MM MD simulation, we have used high-level quantum chemistry calculation to examine the reliability of semiempirical PM3 method using simplified active site model. The geometries were fully optimized with three different basis sets and the corresponding vibrational frequencies were evaluated at the optimized geometries to verify their true stability by use of the Gaussian03 program.[51] Table 3 reveals that the internuclear distances involving zinc determined at different basis set are consistent with each other, and the optimized structure with the 1bsw_water model is closer to the corresponding geometry parameters in the reported X-ray structure, which is in good agreement with results from the QM/ MM MD simulations. The present results obtained from molecular dynamics simulations and quantum chemical calculations strongly support the conclusion that the fourth ligand in the active site of the reported X-ray crystal structure of Acutolysin A is a water molecule rather than a hydroxide ion.

The considerable fluctuations of rmsd in the active site may be followed by tracking key dihedral angles over the course of the simulations as seen in Figure 5, and the average values of these dihedral angles with standard deviations are shown in Table 4. These three dihedral angles involve the coordinate oxygen atom, zinc, nitrogen atoms, and carbon atoms in the imidazole ring of His142, His146, and His152. The definitions of them are specified in the caption of Figure 5, and atom names are also shown in Figure 3. The relatively large fluctuations of these dihedral angles suggest that the imidazole rings are rather flexible. Figure 5 shows that in the 1bsw_water simulation, CE3-NE4-Zn-OH2 (DIHE2) has a relatively large change at about 200 ps, then it quickly changes back to the original conformation until the end of the simulation, while in the 1bsw_hydroxide simulation the dihedral angle of DIHE2 equilibrated to a different conformation which underwent several further inter-conversions. The changes in the dihedral angle of CE3-NE4-Zn-OH2 (DIHE2) for both simulations exhibit similar trends with respect to the rmsd fluctuations of the QM region, and it is the flip of these three imidazole rings that leads to the greatest fluctuation in rmsd. This analysis also shows that the equilibrated structure of 1bsw_water simulation is more consistent with the X-ray crystal structure, so it further supports that the fourth ligand of zinc in the crystal structure is water.

To further examine the rotation of the imidazole rings, we have monitored some hydrogen bonds around them in the second coordination shell (see Figure 6). In the X-ray structure, ND1 and ND3 of QM region (see Figure 3 for atom names) form two hydrogen bonds (HB1 and HB2) with the backbone carbonyl oxygen atoms of Ile165 and Val150, and the formed hydrogen bonds in the active site are shown in Figure 7, a and c, for 1bsw_water and 1bsw_hydroxide systems, respectively. The distances between the corresponding oxygen atom and nitrogen atom are 2.84 Å (HB1) and 2.76 Å (HB2), and thus these groups have quite favorable geometries for hydrogen-bonding interactions. These two hydrogen bonds initially anchor the orientations of the histidine imidazole rings and keep them from rotating too much. But HB2 broke after the short relaxation time, and then a new hydrogen bond (HB3) between ND3 and oxygen of carboxylate group of Glu143 formed. The snapshots with the new formed hydrogen bonds extracted from the MD trajectories are shown in Figure 7, b and d. In the 1bsw_hydroxide simulation, judging from the time order, the new favorable HB3 formed, and this has an obvious impact on the orientations of the other two imidazole rings, which leads to the weakening of the other hydrogen bond (HB1). The distance between the donor and the

acceptor of HB1 has changed from 2.84 Å in the X-ray structure to 3.23 Å, which is the average value over the last 100 ps of simulation as shown in Table 5. In the 1bsw_water simulation as shown in Figure 6a, the HB1 is quite stable and maintained during the entire simulation, which tightly holds the distance between the donor and the acceptor and provides a critical stabilization to the orientation of imidazole ring. With the strong hydrogen-bonding interaction of HB1, it is not surprising that after 300 ps the rebound of conformation is observed. To sum up, in the 1bsw_hydroxide simulation the hydrogen bond network of active site residues changes from the crystal structure of Figure 7c to the conformation of Figure 7d, and that of 1bsw_water simulation changes from the crystal structure of Figure 7a to the conformation of Figure 7b in the beginning of the simulation, then changes back to the conformation of Figure 7a quickly, and keeps the network of Figure 7a to the end of the simulation. Overall, it should be the new hydrogen bond forming and original hydrogen bond breaking, which acts as the anchor for the imidazole ring that induces the torsion of the rings, leading to the big fluctuation of rmsd.

Figure 8 shows the rmsd of Glu143 from the experimental structure. In contrast to the simulation of 1bsw_water, the conformation of Glu143 in the 1bsw_hydroxide system changes substantially after 200 ps. This conformation change is in favor of the new HB3 forming. Thus, it is not surprising that the 1bsw_hydroxide system is equilibrated to another much more different conformation, comparing with the X-ray structure than 1bsw_water system.

In addition, following the suggestions of a reviewer, we added an acetate molecule in the simplified active site model to explore the role of Glu143 in the catalytic mechanism. The geometry was fully optimized using the B3LYP/6-31++G(2d,2p) calculation with Gaussian03, and the optimized structure is shown in Figure 9. From this figure we note that the distances between the two hydrogen atoms and oxygen atom in the catalytic water are 1.49 and 0.97 Å, respectively. Obviously, the catalytic water molecule is polarized by the carboxyl of Glu143, as shown by the difference of 0.52 Å of these two hydrogen–oxygen bonds. In contrast to the lengthened distance between the hydrogen and oxygen atoms in the water, the distance between the carboxyl oxygen atom and hydrogen atom is only 1.04 Å (see Figure 9). The above result is consistent with the proposed mechanism that Glu143 polarizes and accepts a proton from the zinc-bound water ligand through hydrogen bonding, so that it enhances the nucleophilic nature of the water oxygen, and then it might transfer the proton to the leaving NH group of the scissile peptide bond.

To analyze the distribution of water molecules in the active site besides the water coordinated to zinc, we have monitored the movements of all waters within 4.5 Å of zinc in 1bsw_water simulation (Figure 10a). The interesting phenomenon of water molecule exchange is observed during the present 1 ns of simulation time. In the X-ray structure only two crystal waters are found in this sphere (CWAT435 and CWAT372), and after about 100 ps CWAT372 becomes far from zinc. Another water CWAT435 is more stable and stays in the active site for about 650 ps, and then moves away. By observing the residues around this water, we find a hydrogen bond between CWAT435 and backbone carbonyl oxygen of Ala111, which places constraints on the movement of this water before it broke at about 650 ps (see Figure 10b). At about 800 ps, two water molecules (BULK3819 and BULK4047) diffuse into this sphere and form two hydrogen bonds with the backbone carbonyl oxygen of Pro168 and carboxylate group of Glu143. The average values of involved hydrogen bonds are also summarized in Table 5.

Acutolysin A possesses strong hemorrhagic activity with the minimum hemorrhagic dose (MHD) of 0.4 g,59 and its proteolytic activity was observed to be sensitive to pH values, in that the activity under weakly alkaline condition (pH 7.5) is about 100 times stronger than that under weakly acidic condition (pH 5.0).60 Although the present theoretical results indicate that, when there is no substrate and the enzyme cannot function, the fourth ligand of zinc in

the stable X-ray crystal structure is a water molecule, and which one (water or hydroxide) serves as the nucleophile to initialize the hydrolysis of substrate depends upon pH values. Because the hydroxide ion is a better nucleophile than the water molecule,61 the activity of the Acutolysin A catalyzed hydrolysis of the substrate depends on the concentration of the structure form with hydroxide as the fourth ligand of zinc. When the pH of the aqueous solution of Acutolysin A is equal to the kinetic pK_a value of 7.3, which is determined through the experimental pH-rate profile,[60] the concentrations of the two kinds of Acutolysin A active site structures (with hydroxide and with water) should be equal to each other. At lower pH the structural form with water as the fourth ligand should be dominant, and at higher pH the structure form with hydroxide as the fourth ligand should be dominant.[62] So the deprotonation of the zinc-bound water to the better nucleophile of hydroxide under acidic conditions is less facile than that under weakly alkaline condition, which might be the reason why Acutolysin A is inactive or has a low activity under acidic conditions.

Conclusions

Zinc plays an essential role in biological systems, primarily via its function in more than ca. 300 enzymes. However, as a result of the poor spectroscopic properties associated with the Zn^{II} ion, it is a nontrivial issue to determine the structure of the active site of a zinc enzyme in solution.[58] In this work, the identity of the fourth ligand of zinc in Acutolysin A is theoretically determined by performing both combined quantum mechanical and molecular mechanical (QM/MM) simulation and high-level quantum mechanical calculations. The results indicate that the fourth ligand in the active site of the reported X-ray crystal structure is a water molecule rather than a hydroxide anion, and the correct tetrahedral geometry is maintained for zinc throughout the simulation. In the QM/MM simulations, there are considerable fluctuations of rmsd between 200 and 300 ps in the 1bsw_water system and the initial 800 ps in the 1bsw_hydroxide system. Analysis of hydrogen-bonding patterns clearly indicates that the new hydrogen bond forming and original hydrogen bond breaking in the second coordination shell, which plays crucial roles in anchoring imidazole rings, induce the torsion of the rings, leading to the big fluctuation of rmsd. After determination of the identity of the fourth ligand of zinc, the distribution of water molecules within 4.5 Å of zinc in 1bsw_water system has been examined. The exchange of the two crystal waters by another two bulk water is observed in the 1 ns time scale, which is also mentioned by Stote and Karplus.[25] On the basis of these theoretical results, we note that the experimentally observed pH dependence of the proteolytic and hemorrhagic activity of Acutolysin A is because the deprotonation of the zinc-bound water to the better nucleophile of hydroxide under acidic conditions is less facile than that under weakly alkaline condition.

Acknowledgments

We thank the supercomputer center of Virtual Laboratory of Computational Chemistry, Computer Network Information Center, Chinese Academy of Sciences, and the National Institutes of Health (Grant No. GM46736), for the computational resources. We also thank Kwangho Nam and Yao Fan for helpful discussions.

References and Notes

1. Parkin G. Chem. Rev 2004;104:699. [PubMed: 14871139]
2. Auld, DS. Metal Sites in Proteins and Models. Vol. 89. Springer; New York: 1997. Zinc catalysis in metalloproteases.; p. 29
3. Coleman JE. Curr. Opin. Chem. Biol 1998;2:222. [PubMed: 9667939]
4. Lipscomb WN, Strater N. Chem. Rev 1996;96:2375. [PubMed: 11848831]
5. Turner AJ. Biochem. Soc. Trans 2003;31:723. [PubMed: 12773192]
6. Vallee BL, Auld DS. Acc. Chem. Res 1993;26:543.

7. Vallee BL, Auld DS. Biochemistry 1993;32:6493. [PubMed: 8329379]
8. Vallee BL, Auld DS. Proc. Natl. Acad. Sci. U.S.A 1993;90:2715. [PubMed: 8464881]
9. Vallee BL, Falchuk KH. Physiol. Rev 1993;73:79. [PubMed: 8419966]
10. Dudev T, Lim C. Chem. Rev 2003;103:773. [PubMed: 12630852]
11. Zhan CG, de Souza ON, Rittenhouse R, Ornstein RL. J. Am. Chem. Soc 1999;121:7279.
12. Gong WM, Zhu XY, Liu SJ, Teng MK, Niu LW. J. Mol. Biol 1998;283:657. [PubMed: 9784374]
13. Watanabe L, Shannon JD, Valente RH, Rucavado A, Alape-Giron A, Kamiguti AS, Theakston RDG, Fox JW, Gutierrez JM, Arni RK. Protein Sci 2003;12:2273. [PubMed: 14500885]
14. Bjarnason JB, Fox JW. Pharmacol. Ther 1994;62:325. [PubMed: 7972338]
15. Hati R, Mitra P, Sarker S, Bhattacharyya KK. Crit. Rev. Toxicol 1999;29:1. [PubMed: 10066158]
16. Kamiguti AS, Hay CRM, Theakston RDG, Zuzel M. Toxicon 1996;34:627. [PubMed: 8817809]
17. Ownby, CL. Locally-acting agents: Myotoxins, hemorrhagic toxins and dermonecrotic factors.. In: Shier, WT.; Mebs, D., editors. Handbook of toxinology. Marcel Dekker; New York: 1990. p. 601
18. Gutierrez JM, Rucavado A. Biochimie 2000;82:841. [PubMed: 11086214]
19. Liu QD, Xu WH, Cheng X, Liu J. Acta Biochim. Biophys. Sin 2000;32:425. [PubMed: 12075438]
20. Gutierrez JM, Rucavado A, Escalante T, Diaz C. Toxicon 2005;45:997. [PubMed: 15922771]
21. Zhang DC, Botos I, Gomisruth FX, Doll R, Blood C, Njoroge FG, Fox JW, Bode W, Meyer EF. Proc. Natl. Acad. Sci U.S.A 1994;91:8447. [PubMed: 8078901]
22. Hoops SC, Anderson KW, Merz KM. J. Am. Chem. Soc 1991;113:8262.
23. Monard G, Merz KM. Acc. Chem. Res 1999;32:904.
24. Rappe AK, Casewit CJ, Colwell KS, Goddard WA, Skiff WM. J. Am. Chem. Soc 1992;114:10024.
25. Stote RH, Karplus M. Proteins—Struct. Funct. Genet 1995;23:12. [PubMed: 8539245]
26. Nam K, Prat-Resina X, Garcia-Viloca M, Devi-Kesavan LS, Gao J. J. Am. Chem. Soc 2004;126:1369. [PubMed: 14759194]
27. Humphrey W, Dalke A, Schulten K. J. Mol. Graphics 1996;14:33.
28. Amara, P.; Field, MJ. Computational Molecular Biology. Leszczynski, J., editor. Elsevier; Amsterdam: 1999. p. 1
29. Field MJ, Bash PA, Karplus M. J. Comput. Chem 1990;11:700.
30. Gao, J. Reviews in Computational Chemistry. Lipkowitz, KB.; Boyd, DB., editors. Vol. 7. VCH; New York: 1995. p. 119
31. Gao J, Truhlar DG. Annu. Rev. Phys. Chem 2002;53:467. [PubMed: 11972016]
32. MacKerell AD, Bashford D, Bellott M, Dunbrack RL, Evanseck JD, Field MJ, Fischer S, Gao J, Guo H, Ha S, Joseph-McCarthy D, Kuchnir L, Kuczera K, Lau FTK, Mattos C, Michnick S, Ngo T, Nguyen DT, Prodhom B, Reiher WE, Roux B, Schlenkrich M, Smith JC, Stote R, Straub J, Watanabe M, Wiorkiewicz-Kuczera J, Yin D, Karplus M. J. Phys. Chem. B 1998;102:3586.
33. Freindorf M, Gao J. J. Comput. Chem 1996;17:386.
34. Gao, J. Modeling the Hydrogen Bond. American Chemical Society; Washington, DC: 1994. Computation of Intermolecular Interactions with a Combined Quantum-Mechanical and Classical Approach.; p. 8ACS Symposium Series No. 569
35. Stewart JJP. J. Comput. Chem 1989;10:209.
36. Alhambra C, Corchado J, Sanchez ML, Garcia-Viloca M, Gao J, Truhlar DG. J. Phys. Chem. B 2001;105:11326.
37. Alhambra C, Gao J, Corchado JC, Villa J, Truhlar DG. J. Am. Chem. Soc 1999;121:2253.
38. Bash PA, Field MJ, Davenport RC, Petsko GA, Ringe D, Karplus M. Biochemistry 1991;30:5826. [PubMed: 2043624]
39. Devi-Kesavan LS, Gao J. J. Am. Chem. Soc 2003;125:1532. [PubMed: 12568613]
40. Liu HY, MullerPlathe F, vanGunsteren WF. J. Mol. Biol 1996;261:454. [PubMed: 8780786]
41. Truhlar DG, Gao J, Alhambra C, Garcia-Viloca M, Corchado J, Sanchez ML, Villa J. Acc. Chem. Res 2002;35:341. [PubMed: 12069618]
42. Wu RB, Xie HJ, Cao ZX, Mo YR. J. Am. Chem. Soc 2008;130:7022. [PubMed: 18470986]
43. Gao J, Amara P, Alhambra C, Field MJ. J. Phys. Chem. A 1998;102:4714.

44. Jorgensen WL, Chandrasekhar J, Madura JD, Impey RW, Klein ML. J. Chem. Phys 1983;79:926.
45. Brooks BR, Bruccoleri RE, Olafson BD, States DJ, Swaminathan S, Karplus M. J. Comput. Chem 1983;4:187.
46. Hockney RW. Methods Comput. Phys 1970;9:136.
47. Andersen HC. J. Chem. Phys 1980;72:2384.
48. Hoover WG. Phys. Rev. A 1985;31:1695. [PubMed: 9895674]
49. Nosé S. J. Chem. Phys 1984;81:511.
50. Ryckaert J-P, Ciccotti G, Berendsen HJC. J. Comput. Phys 1977;23:327.
51. Frisch, MJ.; Schlegel, HB.; Scuseria, GE.; Robb, MA.; Cheeseman, JR.; Montgomery, JA., Jr.; Vreven, T.; Kudin, KN.; Burant, JC.; Millam, JM.; Iyengar, SS.; Tomasi, J.; Barone, V.; Mennucci, B.; Cossi, M.; Scalmani, G.; Rega, N.; Petersson, GA.; Nakatsuji, H.; Hada, M.; Ehara, M.; Toyota, K.; Fukuda, R.; Hasegawa, J.; Ishida, M.; Nakajima, T.; Honda, Y.; Kitao, O.; Nakai, H.; Klene, M.; Li, X.; Knox, JE.; Hratchian, HP.; Cross, JB.; Adamo, C.; Jaramillo, J.; Gomperts, R.; Stratmann, RE.; Yazyev, O.; Austin, AJ.; Cammi, R.; Pomelli, C.; Ochterski, JW.; Ayala, PY.; Morokuma, K.; Voth, GA.; Salvador, P.; Dannenberg, JJ.; Zakrzewski, VG.; Dapprich, S.; Daniels, AD.; Strain, MC.; Farkas, O.; Malick, DK.; Rabuck, AD.; Raghavachari, K.; Foresman, JB.; Ortiz, JV.; Cui, Q.; Baboul, AG.; Clifford, S.; Cioslowski, J.; Stefanov, BB.; Liu, G.; Liashenko, A.; Piskorz, P.; Komaromi, I.; Martin, RL.; Fox, DJ.; Keith, T.; Al-Laham, MA.; Peng, CY.; Nanayakkara, A.; Challacombe, M.; Gill, PMW.; Johnson, B.; Chen, W.; Wong, MW.; Gonzalez, C.; Pople, JA. Gaussian 03; Revision B.05. Gaussian, Inc.; Pittsburgh, PA: 2003.
52. Becke AD. J. Chem. Phys 1993;98:5648.
53. Lee C, Yang W, Parr RG. Phys. Rev. B 1988;37:785.
54. Dudev T, Lim C. J. Am. Chem. Soc 2000;122:11146.
55. Dudev T, Lim C. J. Phys. Chem. B 2001;105:4446.
56. Dudev T, Lin YL, Dudev M, Lim C. J. Am. Chem. Soc 2003;125:3168. [PubMed: 12617685]
57. Koca J, Zhan CG, Rittenhouse RC, Ornstein RL. J. Am. Chem. Soc 2001;123:817. [PubMed: 11456615]
58. Bergquist C, Fillebeen T, Morlok MM, Parkin G. J. Am. Chem. Soc 2003;125:6189. [PubMed: 12785851]
59. Xu X, Wang C, Liu J, Lu Z. Toxicon 1981;19:633–644. [PubMed: 7302954]
60. Zhu XY, Zhu ZL, Gong WM, Teng MK, Niu LW. Acta Biochim. Biophys. Sin 1997;29:163. [PubMed: 12219222]
61. Zhan CG, Zheng F. J. Am. Chem. Soc 2001;123:2835. [PubMed: 11456970]
62. Zheng F, Zhan CG, Ornstein RL. J. Phys. Chem. B 2002;106:717.

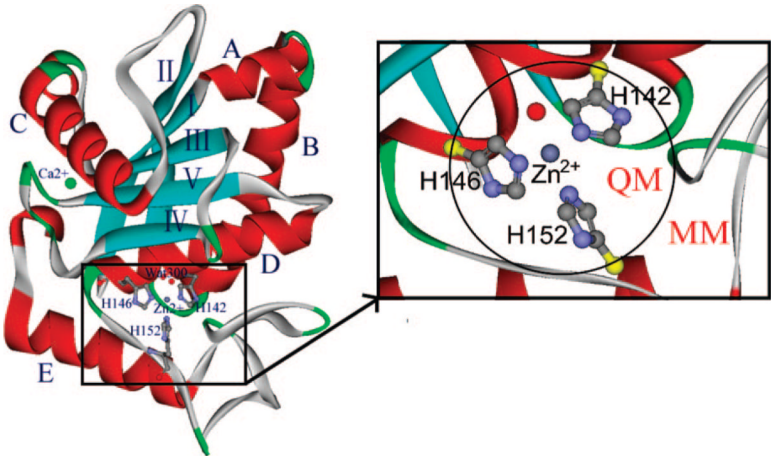

Figure 1.

Left picture is the crystal structure of Acutolysin A from 1bsw.pdb.[12] The molecule is shown in standard orientation. The calcium ion, the zinc ion (filled circles), and the three histidine zinc ligation residues are also shown. The right one is the enlargement for the structure of the active site, and it is also the schematic representation of the partition of the protein system into a quantum mechanical region and a classical region. The boundary atoms are treated using the generalized hybrid orbital method, which are indicated in yellow.

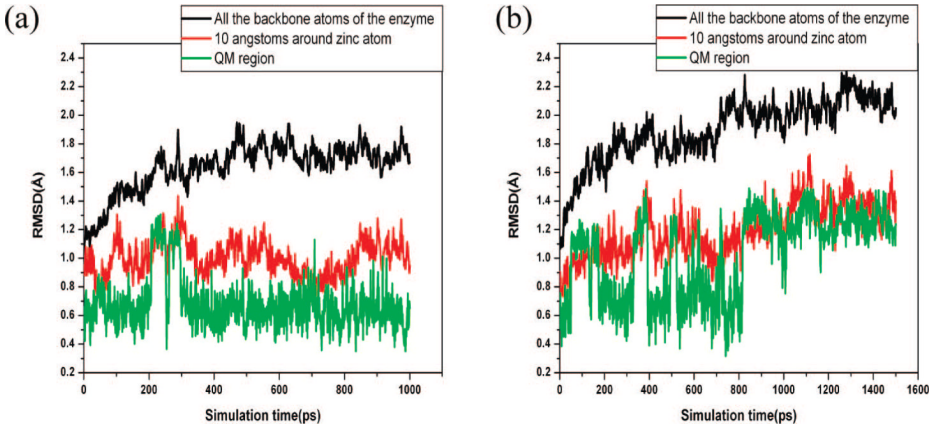

Figure 2.

Root-mean-square deviation (Å) from the experimental structure for backbone atoms, atoms within 10 Å of zinc and atoms in QM region versus the simulation time: (a) for 1bsw_water, (b) for 1bsw_hydroxide.

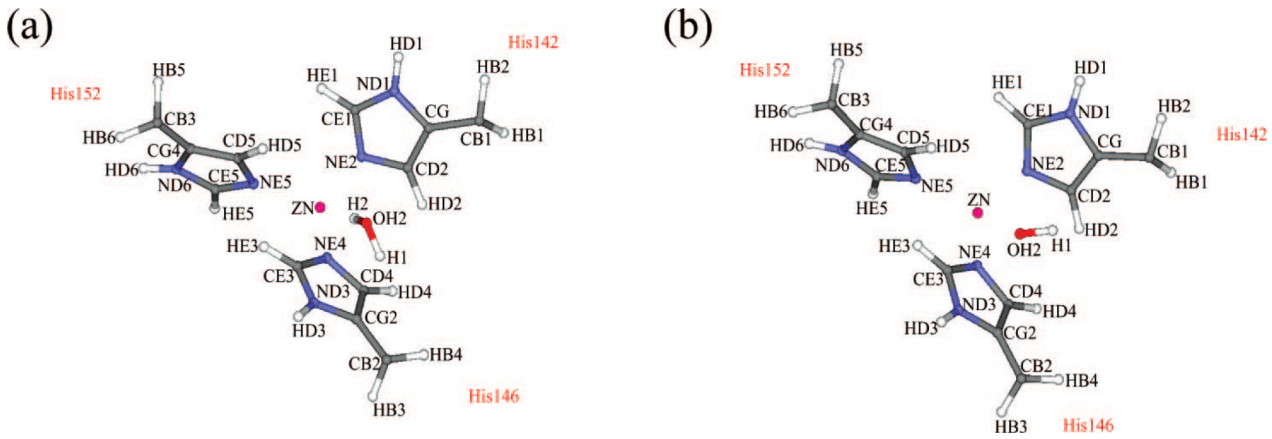

Figure 3.
Definitions of atom names in the active site: (a) for 1bsw_water, (b) for 1bsw_hydroxide.

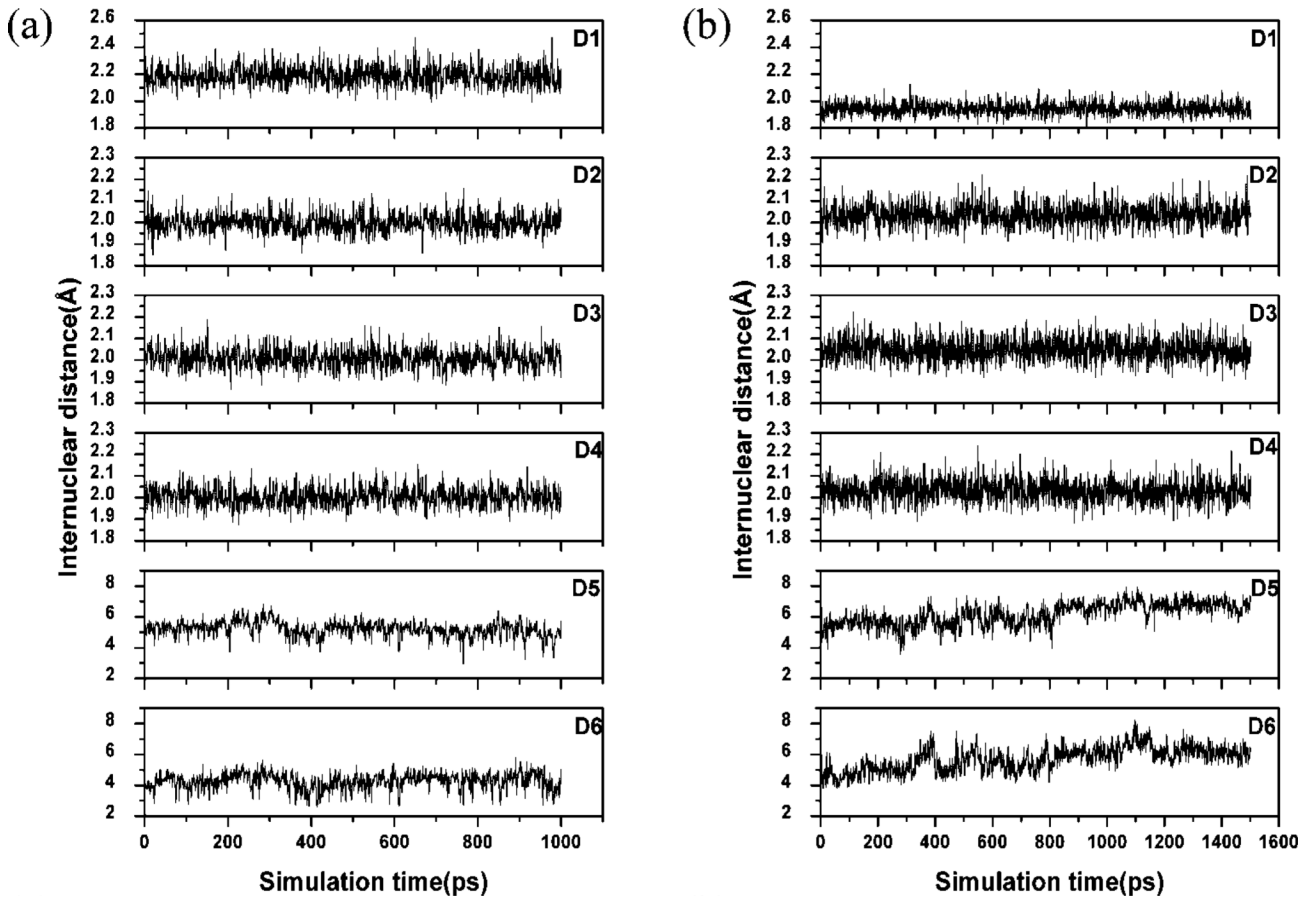

Figure 4.

Selected distances as obtained from MD simulation: (a) for 1bsw_water, (b) for 1bsw_hydroxide. (D1) Zn-OH2 (wat300 or hydroxide ion300), (D2) Zn-His142:NE2, (D3) Zn-His146:NE2, (D4) Zn-His152:NE2, (D5) OH2 (wat300 or hydroxide ion300)-Glu143:OE1, (D6) OH2 (wat300 or hydroxide ion300)-Glu143:OE2. Residue number corresponds to that in the X-ray structure.

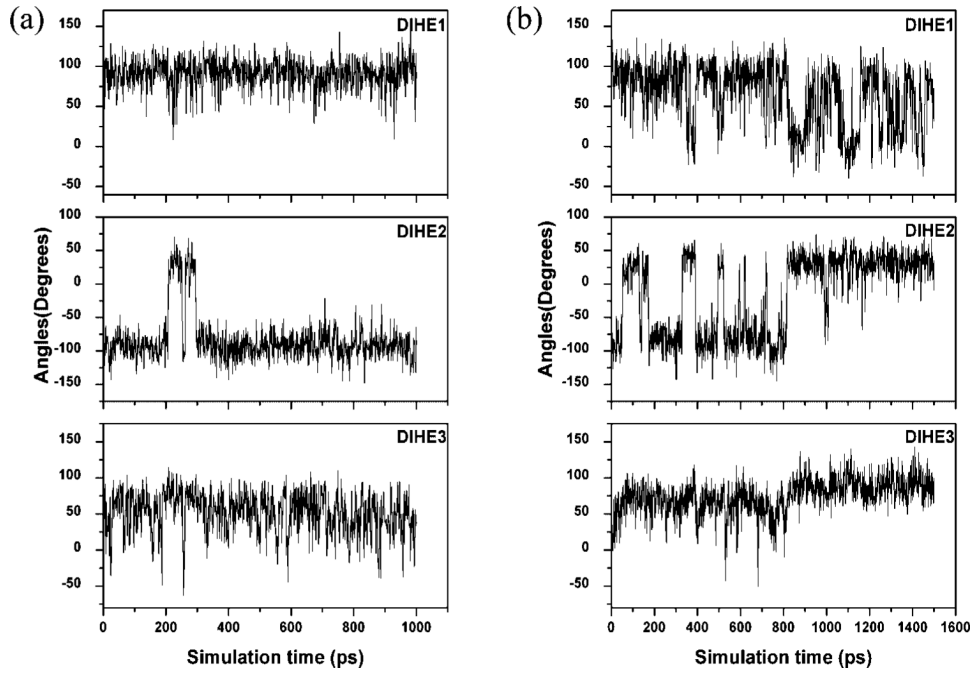

Figure 5.
Selected dihedral angles of atoms in QM region as obtained MD simulation: (a) for 1bsw_water, (b) for 1bsw_hydroxide. (DIHE1) CE1-NE2-Zn-OH2, (DIHE2) CE3-NE4-Zn-OH2, (DIHE3) CE5-NE5-Zn-OH2 (see Figure 3 for atom names).

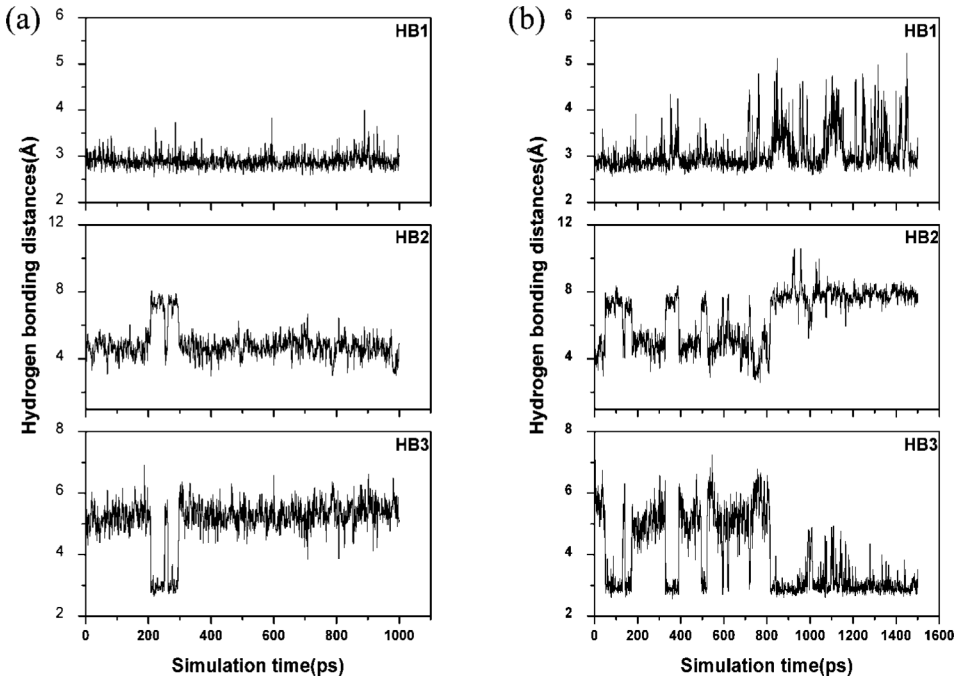

Figure 6.
Selected hydrogen bond distances between donor and acceptor in the active site as obtained from MD simulation: (a) for 1bsw_water, (b) for 1bsw_hydroxide. (HB1) ND1-Ile165:O, (HB2) ND3-Val150:O, (HB3) ND3-Glu143:OE1.

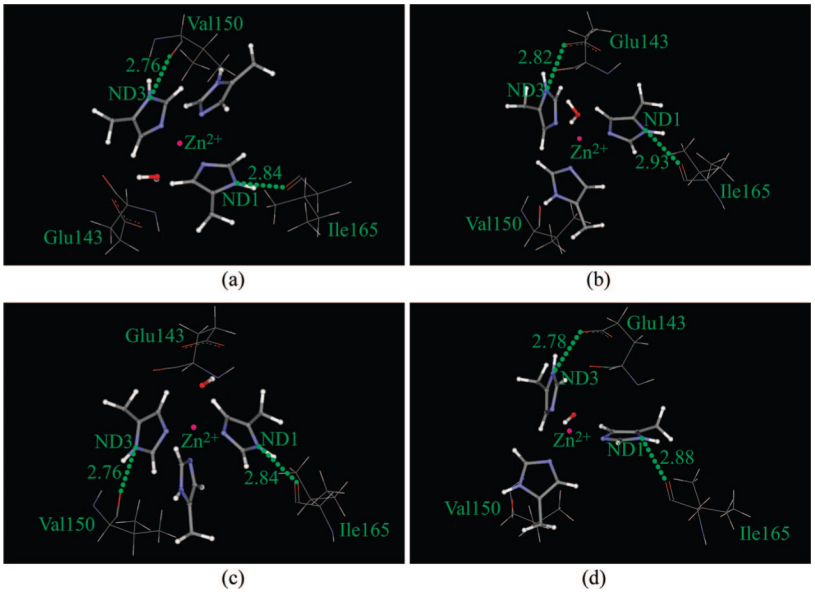

Figure 7.

Hydrogen bonds in the active site: (a) X-ray structure in 1bsw_water, (b) snapshot of 250 ps extracted from MD trajectory in 1bsw_water, (c) X-ray structure in 1bsw_hydroxide, and (d) snapshot of 900 ps extracted from MD trajectory in 1bsw_hydroxide.

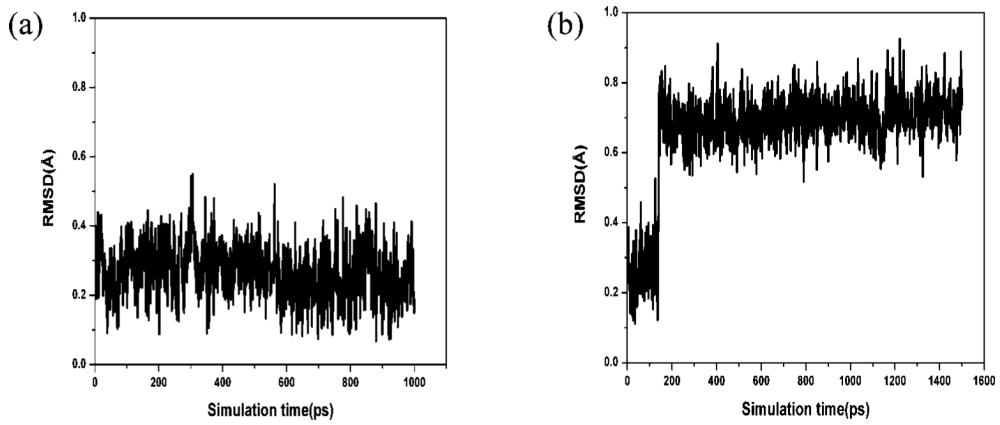

Figure 8.

Root-mean-square deviation (Å) from the experimental structure for the residues of Glu143 in the active site: (a) for 1bsw_water, (b) for 1bsw_hydroxide.

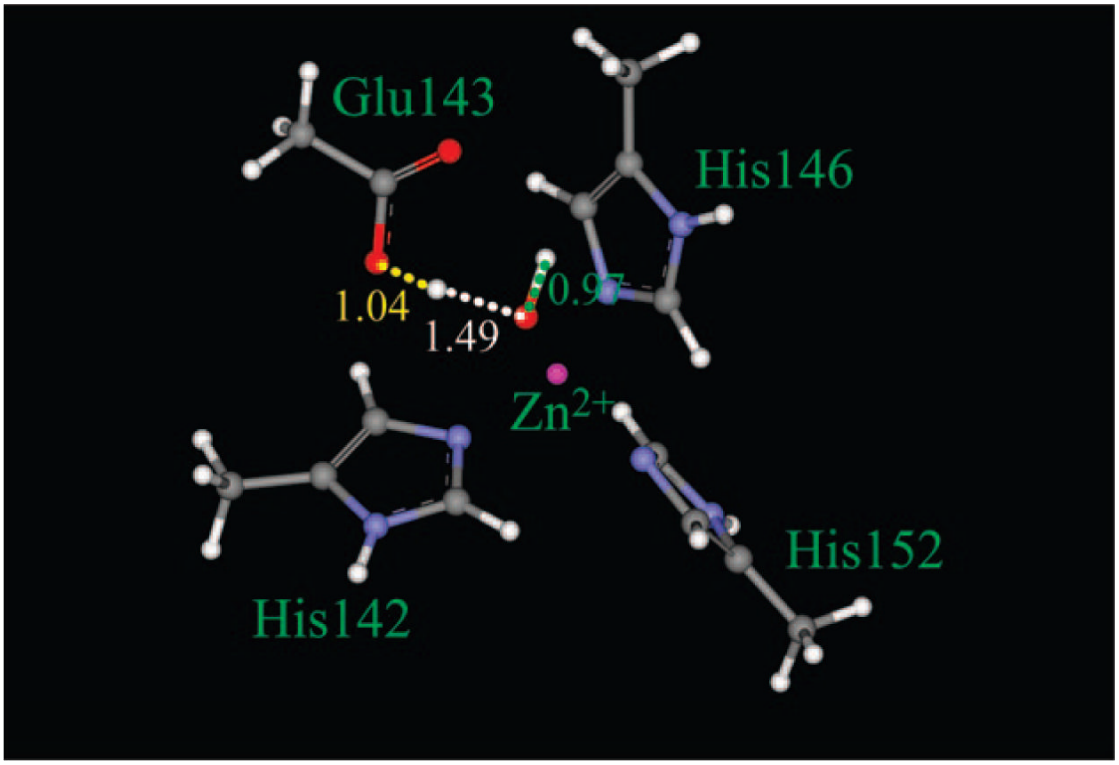

Figure 9.
Optimized structure of active site residues using the high-level QM calculations, which clearly shows the polarization of Glu143 to the catalytic water.

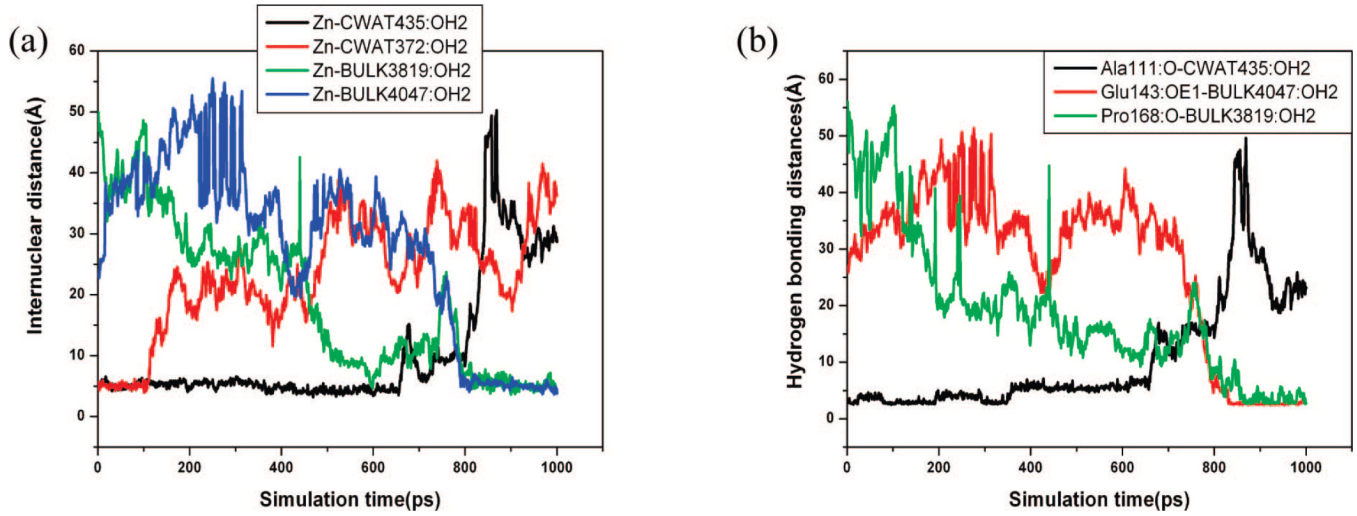

Figure 10.

(a) Plot of distances between zinc and waters in the active site (within 4.5 Å of zinc) versus the simulation time for 1bsw_water. (b) Selected hydrogen bond distances between oxygen atoms of waters in the active site and protein oxygen atoms as obtained from 1bsw_water simulation.

TABLE 1

Experimental and MD Average Values of Selected Distances in the Active Site

distances (Å)	D1	D2	D3	D4	D5	D6
X-ray[a]	2.24	1.99	2.00	1.99	3.73	3.21
1bsw_water	2.18 (0.086[b])	2.00 (0.043)	2.01 (0.047)	2.00 (0.046)	4.87 (0.54)	4.29 (0.66)
1bsw_hydroxide	1.94 (0.047)	2.03 (0.053)	2.03 (0.052)	2.03 (0.052)	6.67 (0.40)	6.05 (0.42)

[a]Values from PDB ID 1BSW.

[b]The values in parentheses are the standard deviations. The definitions of these distances are as follows: (D1) Zn-OH2 (wat300 or hydroxide ion300), (D2) Zn-His142:NE2, (D3) Zn-His146:NE2, (D4) Zn-His152:NE2, (D5) OH2 (wat300 or hydroxide ion300)-Glu143:OE1, (D6) OH2 (wat300 or hydroxide ion300)-Glu143:OE2.

TABLE 2

MD Average Rmsd from the Experimental Structure for Three Atom Sets: Backbone Atoms (S1), Atoms within 10 Å of Zinc (S2) and Atoms in QM Region (S3)

rmsd (Å)	S1	S2	S3
1bsw_water	1.72 (0.067[a])	1.06 (0.082)	0.61 (0.12)
1bsw_hydroxide	2.08 (0.060)	1.33 (0.10)	1.26 (0.091)

[a]The values in parentheses are the standard deviations.

TABLE 3

Values of Selected Distances in the Active Site Calculated at B3LYP Level

	6-31+g(d,p)		6-31++g(d,p)		6-31++g(2d,2p)	
distances (Å)	**1bsw_water**	**1bsw_hydroxide**	**1bsw_water**	**1bsw_hydroxide**	**1bsw_water**	**1bsw_hydroxide**
D1[a]	2.17	1.87	2.16	1.87	2.17	1.87
D2	2.00	2.07	2.00	2.07	1.99	2.07
D3	2.00	2.06	2.00	2.06	1.99	2.06
D4	2.00	2.07	2.00	2.07	2.00	2.07

[a]The definitions of these distances are same as Table 1.

TABLE 4

MD Average Values of Selected Dihedral Angles in the Active Site

dihedral angles (deg)	DIHE1	DIHE2	DIHE3
1bsw_water	92.61(23.88[a])	–94.77 (17.78)	41.86 (26.34)
1bsw_hydroxide	49.26(37.95)	32.44 (17.90)	92.27 (18.18)

[a]The values in parentheses are the standard deviations. The definitions of these dihedral angles are as follows: (DIHE1) CE1-NE2-Zn-OH2, (DIHE2) CCE3-NE4-Zn-OH2, (DIHE3) CE5-NE5-Zn-OH2. (See Figure 3 for atom names.)

TABLE 5

MD Average Values of Selected Hydrogen Bond Distances between Donor and Acceptor in the Active Site[a]

distances (Å)	HB1	HB2	HB3	HB4	HB5
1bsw_water	2.91 (0.20)	4.44 (0.62)	5.46 (0.41)	2.70 (0.16)	3.57 (0.81)
1bsw_hydroxide	3.23 (0.53)	7.86 (0.32)	2.96 (0.21)	–	–

[a]The definitions of these hydrogen bonds are as follows: (HB1) ND1-Ile165:O, (HB2) ND3-Val150:O, (HB3) ND3-Glu143:OE1, (HB4) Glu143:OE1-BULK4047:OH2, (HB5) Pro168:O-BULK-3819:OH2.